Structural Engineering and Mechanics, *Vol. 72, No. 5 (2019) 617-629*
DOI: https://doi.org/10.12989/sem.2019.72.5.617

The linear-elastic stiffness matrix model analysis of pre-twisted Euler-Bernoulli beam

Ying Huang[1,2a], Haoran Zou[3b], Changhong Chen[*3], Songlin Bai[3d], Yao Yao[3c] and Leon M. Keer[4e]

[1]*School of Civil Engineering, Xi'an University of Architecture and Technology, Xi'an, China, 710055, China*
[2]*Key Lab of Structural Engineering and Earthquake Resistance, Ministry of Education (XAUAT), Xi'an, 710055, China*
[3]*School of Mechanics and civil Engineering, Northwestern Polytechnical University, Xi'an, China, 710129, China*
[4]*Civil and Environmental Engineering, Northwestern University, Evanston, IL, 60286, U.S.A.*

(Received February 18, 2019, Revised April 16, 2019, Accepted July 30, 2019)

Abstract. Based on the finite element method of traditional straight Euler-Bernoulli beams and the coupled relations between linear displacement and angular displacement of a pre-twisted Euler-Bernoulli beam, the shape functions and stiffness matrix are deduced. Firstly, the stiffness of pre-twisted Euler-Bernoulli beam is developed based on the traditional straight Euler-Bernoulli beam. Then, a new finite element model is proposed based on the displacement general solution of a pre-twisted Euler-Bernoulli beam. Finally, comparison analyses are made among the proposed Euler-Bernoulli model, the new numerical model based on displacement general solution and the ANSYS solution by Beam188 element based on infinite approach. The results show that developed numerical models are available for the pre-twisted Euler-Bernoulli beam, and which provide more accurate finite element model for the numerical analysis. The effects of pre-twisted angle and flexural stiffness ratio on the mechanical property are investigated.

Keywords: Pre-twisted; Euler-Bernoulli beam; Stiffness matrix; Parametric analysis

1. Introduction

The pre-twisted beam, also known as a naturally twisted beam, presents an initially twisted shape in the natural state. Pre-twisted beams are widely used as structural elements. The blades of propellers, turbines and fans and drill bits are usually modelled as pre-twisted beams. Pre-twisted thin-walled members are being increasingly used in the construction of steel structure buildings and bridges. Based on the change rule of the pre-twisted angle along the beam axis, the pre-twisted beam can be divided into two cases (Zupan and Saje 2004): 1) Linear pre-twisted beam; 2) Non-linear pre-twisted beam.

Based on the shape feature, the pre-twisted beam can be defined as the nth order pre-twisted beam when the pre-twisted angle ω is in the range of $((n-1)\pi, n\pi)$, $(n=1,2,\ldots)$, as shown in Fig.1. Since a pre-twisted beam with small pre-twisted angle is dominant in application of civil engineering structures, the first order pre-twisted beam will be discussed in this paper, i.e. pre-twisted angle is in the range of $(0, 0.5\pi]$.

The early literature mainly focused on stress analysis of pre-twisted rod. Berdichevskii *et al*. (1985) investigated thestress state of a pre-twisted rod, and showed that the spatial problem can be successfully reduced to a Neumann-type problem for a certain system of second-order elliptic equations in the cross-section. The research of pre-twisted rod was decomposed into two independent problems, one bending and one extension-torsion.

Recent research is focused on studying the vibration performance of pre-twisted blades and beams by using different techniques. A carefully selected sample of the relevant literature are as follows: Yoo *et al*. (2001) used a modeling method for the vibration analysis of rotating pre-twisted blades with a concentrated mass. Banerjee (2001, 2004) developed an exact dynamic stiffness method to predict the natural frequencies of a pre-twisted beam. Choi *et al*. (2007) studied bending vibration control of the pre-twisted rotating composite thin-walled beam based on a single cell composite beam. Sinha *et al*. (2011) derived the governing partial differential equation of motion for the transverse deflection of a rotating pre-twisted plate by using the thin shell theory. Chen *et al*. (2019) presented a new dynamic model based on the shell theory to investigate the vibration behavior of a rotating composite laminated blade with a pre-twisted angle. Yao *et al*. (2019) established a rotating pre-twisted cylindrical shell model with a

∗Corresponding author, Associate Professor
E-mail: changhong.chen@nwpu.edu.cn
[a] Associate Professor
E-mail: cch-by@163.com
[b] M.Sc. Student
E-mail: zouhaoran@mail.nwpu.edu.cn
[c] Professor
E-mail: yaoy@nwpu.edu.cn
[d] M.Sc. Student
E-mail: 2014301504@mail.nwpu.edu.cn
[e] Professor
E-mail: l-keer@northwestern.edu

ISSN: 1225-4568 (Print), 1598-6217 (Online)

(a) $\omega = \pi / 2$ (b) $\omega = \pi$ (c) $\omega = 2\pi$

Fig.1 the beam model with different pre-twisted angle

presetting angle to investigate nonlinear dynamic responses of the aero-engine compressor blade. Based on the first-order shear deformation theory and the isotropic constitutive law, nonlinear partial differential governing equations are derived by using the Hamilton principle. Zhang *et al*. (2019) presented an investigation to reveal the primary resonance of a rotating pre-twisted blade subject to a flapwise natural frequency gas excitation under thermal gradient in the presence of 2:1 internal resonance. The amplitude-frequency relationships are examined with the focus on the effects of thermal gradient, pre-deformation amplitude, rotating speed, gas pressure and damping coefficients. The post-buckling and coupled bi-directional transverse-longitudinal free vibration behavior of post-buckled rotating pre-twisted functionally graded (FG) microbeams in thermal environment are presented (Shenas *et al*. 2017, 2019). Adair *et al*. (2018) made vibration analysis of a uniform pre-twisted rotating Euler–Bernoulli beam using the modified Adomian decomposition method. Bahaadini, R. and Saidi, A. R. (2019) carried aero-thermoelastic flutter analysis of pre-twisted thin-walled rotating blades reinforced with functionally graded carbon nanotubes. Oh, Y *et al*. (2018) considered the coupling effects of stretching, bending, and torsion to analyze a rotating pre-twisted blade. Lee, J. Y. (2016) considered the Effect of Rotary Inertia Using the Transfer matrix method to develop a vibration analysis for the Pre-twisted Beam. Mohanty *et al*. (2015) analyzed the vibration and dynamic stability of pre-twisted thick cantilever beam made of functionally graded material. Wang *et al*. (2018) made a three-dimensional vibration analysis of curved and twisted beams with irregular shapes of cross-sections by sub-parametric quadrature element method.

The finite element technique has also been applied by many investigators, mostly for the vibration analysis of beams of uniform cross-section. All these investigations differ from one another in the nodal degrees of freedom taken for deriving the element stiffness and mass matrices. Chen and Keer (1993) studied the transverse vibration problems of a rotating twisted Timoshenko beam under axial loading and spinning about its axial axis, and investigated the effects of the twist angle, rotational speed, and axial force on natural frequencies by the finite element method. Nabi and Ganesan (1996) analyzed the vibration characteristics of pre-twisted metal matrix composite blades by using beam and plate theories. A beam element with eight degrees of freedom per node has been developed with torsion-flexure, flexure-flexure and shear-flexure couplings, which are encountered in twisted composite beams. A triangular plate element was used for the composite material to model the beam as a plate structure. Rao and Gupta (2001) derived the stiffness and mass matrices of a rotating twisted and tapered Timoshenko beam element, and calculated the first four natural frequencies and mode shapes in the bending–bending mode for cantilever beams.

However, only a few works have been reported in the existing literature on finite element formulation of pre-twisted beam based on coupled displacement fields (Tabarrok and Farshad 1988, Chen *et al*. 2014, Chen *et al*. 2016, Huang *et al*. 2019, 2017). The common finite element method to handle the static and dynamic problems of the pre-twisted beam is based on infinite approach strategy (ANSYS Inc. 2016). However, the polynomial displacement functions based on traditional straight beam do not correctly reflect the fact that the strain is zero when rigid motion occurs. Moreover, the fact that bending displacements are coupled with each other due to the naturally twisted angle ω will further cause new discretization error. Therefore, in the present study, two new finite element models based on the coupling bending displacements and displacement general solution of pre-twisted Euler-Bernoulli beam are developed.

2. The stiffness of pre-twisted Euler-Bernoulli beam element

2.1 The displacement functions

The following assumptions are adopted based on the traditional straight Euler-Bernoulli beam:

(1) The cross-section shape is unchanged;
(2) Only shear deformation is considered by constraining torsion and ignoring shear deformation for the lateral load;
(3) The deformation is small and linear elastic;
(4) The coupling effects between the various deformations are not considered.

In the local coordinate system G_ξηz, the Euler-Bernoulli beam element is two nodes with twelve degrees of freedom, as shown in Fig. 2. The element length is l, and the parameter k denotes the pre-twisted angle rate ($k = \frac{\mathrm{d}\omega}{\mathrm{d}z} = \omega / l$). Each node has six displacement vectors, namely, u, v, w, φ_ξ, φ_η and φ_z respectively. Each node has also six force vectors, namely, Q_ξ, Q_η, N, M_ξ, M_η and M_z, respectively. The axial displacement w uses a Lagrange interpolation function of two nodes, regardless of the effect of biaxial bending displacement. The bending displacement u and v use the cubic polynomial interpolation function. The torsional angular displacement also uses the two-node Lagrange interpolation function. The specific expression is as follows

$$\begin{cases} u = a_0 + a_1 z + a_2 z^2 + a_3 z^3 \\ v = b_0 + b_1 z + b_2 z^2 + b_3 z^3 \\ w = c_0 + c_1 z \\ \varphi_z = d_0 + d_1 z \end{cases} \tag{1}$$

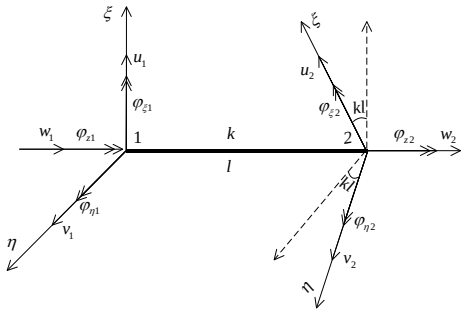

Fig. 2 The node displacements of pre-twisted Euler-Bernoulli beam

where the parameters a_i, b_i (i=0,1,2,3), c_i and d_i (i=0,1) are undetermined coefficients, respectively.

According to the assumption (2) and literature (Banerjee 2004, Chen *et al*. 2014, Chen *et al*. 2016), the equation relating linear displacement and angle displacement is as the follows

$$\frac{\mathrm{d}u}{\mathrm{d}z}=\varphi_\eta+kv\ ,\ \frac{\mathrm{d}v}{\mathrm{d}z}=-\varphi_\xi-ku \tag{2}$$

The displacement interpolation functions can then be expressed as the following

$$\begin{cases} u=a_0+a_1z+a_2z^2+a_3z^3 \\ v=b_0+b_1z+b_2z^2+b_3z^3 \\ w=c_0+c_1z \\ \varphi_\xi=-ku-\dfrac{\mathrm{d}v}{\mathrm{d}z} \\ \varphi_\eta=\dfrac{\mathrm{d}u}{\mathrm{d}z}-kv \\ \varphi_z=d_0+d_1z \end{cases} \tag{3}$$

Introducing the boundary conditions

$$\begin{cases} u\big|_{z=0}=u_1,\ v_{z=0}=v_1,\ w\big|_{z=0}=w_1,\ \varphi_\xi\big|_{z=0}=\varphi_{\xi1} \\ \varphi_\eta\big|_{z=0}=\varphi_{\eta1},\ \varphi_z\big|_{z=0}=\varphi_{z1} \\ u\big|_{z=l}=u_2,\ v_{z=l}=v_2,\ w\big|_{z=l}=w_2,\ \varphi_\xi\big|_{z=l}=\varphi_{\xi2} \\ \varphi_\eta\big|_{z=l}=\varphi_{\eta2},\ \varphi_z\big|_{z=l}=\varphi_{z2} \end{cases} \tag{4}$$

the equation (3) can be further expressed into matrix form, as follows

$$\boldsymbol{u}=\boldsymbol{N}\cdot\boldsymbol{u}_e \tag{5}$$

where the displacement vector is: $\boldsymbol{u}=[u\ v\ w\ \varphi_\xi,\ \varphi_\eta\ \varphi_z]^T$. The nodal displacement is

$$\boldsymbol{u}_e=\begin{bmatrix} u_1 & v_1 & w_1 & \varphi_{\xi1} & \varphi_{\eta1} & \varphi_{z1} & u_2 & v_2 & w_2 & \varphi_{\xi2} & \varphi_{\eta2} & \varphi_{z2} \end{bmatrix}^T$$

The shape function matrix $\boldsymbol{N}$ is as follows

$$\boldsymbol{N}=\begin{bmatrix} \mathbf{N}_1 \\ \mathbf{N}_2 \\ \mathbf{N}_3 \\ \mathbf{N}_4 \\ \mathbf{N}_5 \\ \mathbf{N}_6 \end{bmatrix}=\left[\begin{array}{cccccc|cccccc} N_1 & N_3 & 0 & 0 & N_7 & 0 & N_2 & N_4 & 0 & 0 & N_8 & 0 \\ -N_3 & N_1 & 0 & -N_7 & 0 & 0 & -N_4 & N_2 & 0 & -N_8 & 0 & 0 \\ 0 & 0 & N_5 & 0 & 0 & 0 & 0 & 0 & N_6 & 0 & 0 & 0 \\ -kN_1+\dfrac{\mathrm{d}N_3}{\mathrm{d}z} & -kN_3-\dfrac{\mathrm{d}N_1}{\mathrm{d}z} & 0 & \dfrac{\mathrm{d}N_7}{\mathrm{d}z} & -kN_7 & 0 & -kN_2+\dfrac{\mathrm{d}N_4}{\mathrm{d}z} & -kN_4-\dfrac{\mathrm{d}N_2}{\mathrm{d}z} & 0 & \dfrac{\mathrm{d}N_8}{\mathrm{d}z} & -kN_8 & 0 \\ kN_3+\dfrac{\mathrm{d}N_1}{\mathrm{d}z} & -kN_1+\dfrac{\mathrm{d}N_3}{\mathrm{d}z} & 0 & kN_7 & \dfrac{\mathrm{d}N_7}{\mathrm{d}z} & 0 & kN_4+\dfrac{\mathrm{d}N_2}{\mathrm{d}z} & -kN_2+\dfrac{\mathrm{d}N_4}{\mathrm{d}z} & 0 & kN_8 & \dfrac{\mathrm{d}N_8}{\mathrm{d}z} & 0 \\ 0 & 0 & 0 & 0 & 0 & N_9 & 0 & 0 & 0 & 0 & 0 & N_{10} \end{array}\right]$$

where

$$N_1=(2z+l)(l-z)^2/l^3,\ N_2=z^2(3l-2z)/l^3,$$
$$N_3=kz(l-z)^2/l^2,\ N_4=-kz^2(l-z)/l^2\ N_7=z(l-z)^2/l^2,$$
$$N_8=-z^2(l-z)/l^2,\ N_5=N_9=(l-z)/l,\ N_6=N_{10}=z/l$$

2.2 The element stiffness matrix

According to the assumption (4), the axial tensile strain energy of the pre-twisted Euler-Bernoulli beam is as follows

$$U_a=\frac{1}{2}EA\int_0^l\varepsilon^2\mathrm{d}z=\frac{1}{2}EA\int_0^l\left(\frac{\mathrm{dw}}{\mathrm{d}z}\right)^2\mathrm{d}z \tag{6}$$

where EA is axial stiffness. Introducing the shape function, the equation (6) can be expressed as

$$U_a=\frac{1}{2}\boldsymbol{u}_e^T\cdot EA\int_0^l\left(\frac{\mathrm{d}\mathbf{N}_3}{\mathrm{d}z}\right)^T\left(\frac{\mathrm{d}\mathbf{N}_3}{\mathrm{d}z}\right)\mathrm{d}z\cdot\boldsymbol{u}_e \tag{7}$$

Similarly, the strain energy caused by torsion of the pre-twisted Euler-Bernoulli beam is

$$U_t=\frac{1}{2}\boldsymbol{u}_e^T\cdot GJ\int_0^l\left(\frac{\mathrm{d}\mathbf{N}_6}{\mathrm{d}z}\right)^T\left(\frac{\mathrm{d}\mathbf{N}_6}{\mathrm{d}z}\right)\mathrm{d}z\cdot\boldsymbol{u}_e \tag{8}$$

where GJ is the shear stiffness. According to the assumption (2) and the equations of axial strain caused by biaxial bending (Banerjee 2004, Chen *et al*. 2014, Chen *et al*. 2016), as follows

$$\varepsilon_{z\_\xi}=\eta(\varphi_\xi^{'}-k\varphi_\eta) \tag{9}$$

$$\varepsilon_{z\_\eta}=-\xi(\varphi_\eta^{'}+k\varphi_\xi) \tag{10}$$

The biaxial bending strain energy of the pre-twisted Euler-Bernoulli beam is:

$$U_\mathrm{b}=\frac{1}{2}E\int_0^l\int_A(\varepsilon_{z\_\xi}+\varepsilon_{z\_\eta})^2\mathrm{d}A\mathrm{d}z \tag{11}$$

Introducing the shape function, the biaxial bending strain energy is

$$\begin{aligned} U_b=&\frac{1}{2}\boldsymbol{u}_e^T\cdot\left[EI_\xi\int_0^l\left(\frac{\mathrm{d}^2\mathbf{N}_2}{\mathrm{d}z^2}+2k\frac{\mathrm{d}\mathbf{N}_1}{\mathrm{d}z}-k^2\mathbf{N}_2\right)^T\left(\frac{\mathrm{d}^2\mathbf{N}_2}{\mathrm{d}z^2}+2k\frac{\mathrm{d}\mathbf{N}_1}{\mathrm{d}z}-k^2\mathbf{N}_2\right)\mathrm{d}z\right]\cdot\boldsymbol{u}_e \\ &+\frac{1}{2}\boldsymbol{u}_e^T\cdot\left[EI_\eta\int_0^l\left(\frac{\mathrm{d}^2\mathbf{N}_1}{\mathrm{d}z^2}-2k\frac{\mathrm{d}\mathbf{N}_2}{\mathrm{d}z}-k^2\mathbf{N}_1\right)^T\left(\frac{\mathrm{d}^2\mathbf{N}_1}{\mathrm{d}z^2}-2k\frac{\mathrm{d}\mathbf{N}_2}{\mathrm{d}z}-k^2\mathbf{N}_1\right)\mathrm{d}z\right]\cdot\boldsymbol{u}_e \end{aligned} \tag{12}$$

where EI_ξ and EI_η are the flexural stiffness in the local coordinate system G_ξηz. According to equations (7), (8)

and (12), the element stiffness matrix of a pre-twisted Euler-Bernoulli beam in the local coordinate is as follows

$$\begin{aligned}\mathbf{K}^e = {} & EA\int_0^l \left(\frac{\mathrm{d}\mathbf{N}_3}{\mathrm{d}z}\right)^T\left(\frac{\mathrm{d}\mathbf{N}_3}{\mathrm{d}z}\right)\mathrm{d}z + GJ\int_0^l \left(\frac{\mathrm{d}\mathbf{N}_6}{\mathrm{d}z}\right)^T\left(\frac{\mathrm{d}\mathbf{N}_6}{\mathrm{d}z}\right)\mathrm{d}z \\ & + EI_\xi\int_0^l \left(\frac{\mathrm{d}^2\mathbf{N}_2}{\mathrm{d}z^2}+2k\frac{\mathrm{d}\mathbf{N}_1}{\mathrm{d}z}-k^2\mathbf{N}_2\right)^T\left(\frac{\mathrm{d}^2\mathbf{N}_2}{\mathrm{d}z^2}+2k\frac{\mathrm{d}\mathbf{N}_1}{\mathrm{d}z}-k^2\mathbf{N}_2\right)\mathrm{d}z \\ & + EI_\eta\int_0^l \left(\frac{\mathrm{d}^2\mathbf{N}_1}{\mathrm{d}z^2}-2k\frac{\mathrm{d}\mathbf{N}_2}{\mathrm{d}z}-k^2\mathbf{N}_1\right)^T\left(\frac{\mathrm{d}^2\mathbf{N}_1}{\mathrm{d}z^2}-2k\frac{\mathrm{d}\mathbf{N}_2}{\mathrm{d}z}-k^2\mathbf{N}_1\right)\mathrm{d}z\end{aligned} \quad (13)$$

The specific expression of pre-twisted Euler-Bernoulli beam can be seen in appendix A. If the pre-twisted angle rate k is assumed to be zero (k=0), then the element stiffness matrix is the same as the traditional straight beam; i.e., the pre-twisted beam will be degenerated to a traditional straight beam.

3. A new stiffness matrix model based on displacement general solution

3.1 The displacement functions

The pre-twisted Euler-Bernoulli beam element model, whose length is l and the pre-twisted angle rate is k, is studied in the local coordinate system G_ξηz, as shown in Fig.3. When the node is i, the displacements are u_i, v_i, w_i, $\varphi_{\xi i}$, $\varphi_{\eta i}$ and φ_{zi}, respectively. The displacements are u_{i+1}, v_{i+1}, w_{i+1}, $\varphi_{\xi i+1}$, $\varphi_{\eta i+1}$, φ_{zi+1} when node is i+1, respectively.

Assuming the pre-twisted element is constant strain element, the general displacement solution of the pre-twisted Euler-Bernoulli beam is used as the displacement interpolation functions (Yu and Ma 2002), as follows

$$\begin{aligned}[U] &= [A]\begin{Bmatrix}[U_0]-[\Omega_R][\varphi_0] \\ +\int_{z_i}^{z}[A]^T[\varepsilon]\mathrm{d}z-[\Omega_R]\int_{z_i}^{z}[A]^T[K]\,\mathrm{d}z \\ +\int_{z_i}^{z}[\Omega_R][A]^T[K]\mathrm{d}z\end{Bmatrix} \\ [\varphi] &= [A][\varphi_0]+[A]\int_{z_i}^{z}[A]^T[K]\mathrm{d}z\end{aligned} \quad (14)$$

where

$$[A]=\begin{bmatrix}1 & 0 & 0\\ 0 & \cos kz & \sin kz\\ 0 & -\sin kz & \cos kz\end{bmatrix},$$

which is the coordinate transformation matrix. $[U_0]$, $[\varphi_0]$, $[K]$ and $[\varepsilon]$ are undetermined constant strain vectors, respectively; $[\Omega_R]$ is the dual-antisymmetric matrix generated by the vector $[R]=[Z]-[Z_i]$; $[Z_i]$ represents position vector $[Z]$ when $z=z_i$, namely $[Z_i]=[Z]_{z=zi}$.

When z is equal to z_i, the equation (14) can be simplified to the following

$$[U_0]=[A_i]^T[U_i],\ [\varphi_0]=[A_i]^T[\varphi_i] \quad (15)$$

where $[U_i]=[U]_{z=zi}$, $[\varphi_i]=[\varphi]_{z=zi}$, $[A_i]=[A]_{z=zi}$.

When z is equal to z_{i+1}, the equation (14) can be simplified to the following

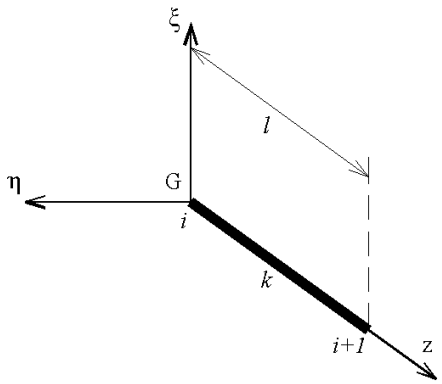

Fig. 3 the element of pre-twisted Euler-Bernoulli beam

$$\begin{aligned}&[A_{i+1}]^T[U_{i+1}]-[A_i]^T[U_i]+[\Omega_{R_{i+1}}][A_i]^T[\varphi_i] \\ &=\int_{z_i}^{z_{i+1}}[A]^T[\varepsilon]\mathrm{d}z \\ &+\int_{z_i}^{z_{i+1}}[\Omega_R][A]^T[K]\mathrm{d}z-[\Omega_{R_{i+1}}]\int_{z_i}^{z_{i+1}}[A]^T[K]\mathrm{d}z\end{aligned} \quad (16)$$

$$[A_{i+1}]^T[\varphi_{i+1}]-[A_i]^T[\varphi_i]=\int_{z_i}^{z_{i+1}}[A]^T[K]\mathrm{d}z \quad (17)$$

where $[\Omega_{R_{i+1}}]$ is the dual-antisymmetric matrix generated by the vector $[R_{i+1}]=[Z_{i+1}]-[Z_i]$.

The constant strain matrix $[K]$ is obtained by the equation (17), as follows

$$[K]=(\int_{z_i}^{z_{i+1}}[A]^T\mathrm{d}z)^{-1}([A_{i+1}]^T[\varphi_{i+1}]-[A_i]^T[\varphi_i]) \quad (18)$$

Substituting (18) into (16), the following equation (19) can be obtained

$$\begin{aligned}&[A_{i+1}]^T[U_{i+1}]-[A_i]^T[U_i]+[\Omega_{R_{i+1}}][A_{i+1}]^T[\varphi_{i+1}] \\ &=\int_{z_i}^{z_{i+1}}[A]^T[\varepsilon]\mathrm{d}z+\int_{z_i}^{z_{i+1}}[\Omega_R][A]^T[K]\mathrm{d}z\end{aligned} \quad (19)$$

The constant strain matrix $[\varepsilon]$ is obtained by substituting (18) into (19), as

$$[\varepsilon]=\begin{bmatrix}[T_{11}] & [T_{12}] & [T_{13}] & [T_{14}]\end{bmatrix}\cdot\begin{bmatrix}[U_i]\\ [\varphi_i]\\ [U_{i+1}]\\ [\varphi_{i+1}]\end{bmatrix} \quad (20)$$

where

$$[T_{11}]=-\left(\int_{z_i}^{z_{i+1}}[A]^T\mathrm{d}z\right)^{-1}[A_i]^T$$

$$[T_{12}]=\left(\int_{z_i}^{z_{i+1}}[A]^T\mathrm{d}z\right)^{-1}\int_{z_i}^{z_{i+1}}[\Omega_R][A]^T\left(\int_{z_i}^{z_{i+1}}[A]^T\mathrm{d}z\right)^{-1}[A_i]^T\mathrm{d}z$$

$$[T_{13}]=\left(\int_{z_i}^{z_{i+1}}[A]^T\mathrm{d}z\right)^{-1}[A_{i+1}]^T$$

$$[T_{14}]=\left(\int_{z_i}^{z_{i+1}}[A]^T\mathrm{d}z\right)^{-1}\begin{Bmatrix}[\Omega_{R_{i+1}}][A_{i+1}]^T \\ -\int_{z_i}^{z_{i+1}}[\Omega_R][A]^T\left(\int_{z_i}^{z_{i+1}}[A]^T\mathrm{d}z\right)^{-1}[A_{i+1}]^T\mathrm{d}z\end{Bmatrix}$$

Similarly, equation (18) can be expressed by node displacements as

$$[K]=\begin{bmatrix}[T_{21}] & [T_{22}] & [T_{23}] & [T_{24}]\end{bmatrix}\cdot\begin{bmatrix}[U_i]\\ [\varphi_i]\\ [U_{i+1}]\\ [\varphi_{i+1}]\end{bmatrix} \tag{21}$$

where

$[T_{21}]=[0]$

$[T_{22}]=-\left(\int_{z_i}^{z_{i+1}}[A]^T\,\mathrm{d}z\right)^{-1}[A_i]^T$

$[T_{23}]=[0]$

$[T_{24}]=\left(\int_{z_i}^{z_{i+1}}[A]^T\,\mathrm{d}z\right)^{-1}[A_{i+1}]^T$

The total constant strain matrix is by the equations (20) and (21)

$$\begin{bmatrix}\varepsilon\\ K\end{bmatrix}=[T]\cdot\begin{bmatrix}[U_i]\\ [\varphi_i]\\ [U_{i+1}]\\ [\varphi_{i+1}]\end{bmatrix} \tag{22}$$

where $[T]=\begin{bmatrix}[T_{11}] & [T_{12}] & [T_{13}] & [T_{14}]\\ [T_{21}] & [T_{22}] & [T_{23}] & [T_{24}]\end{bmatrix}$.

The displacement function can be obtained by substituting equation (22) into equation (14), as follows

$$\begin{bmatrix}[U]\\ [\varphi]\end{bmatrix}=[N]\cdot\begin{bmatrix}[U_i]\\ [\varphi_i]\\ [U_{i+1}]\\ [\varphi_{i+1}]\end{bmatrix} \tag{23}$$

where the shape function is

$$[N]=\begin{bmatrix}[N_{11}] & [N_{12}] & [N_{13}] & [N_{14}]\\ [N_{21}] & [N_{22}] & [N_{23}] & [N_{24}]\end{bmatrix} \tag{24}$$

where

$[N_{11}]=[A]\left([A_i]^T+[T_{11}]\int_{z_i}^{z}[A]^T\,\mathrm{d}z\right)$

$[N_{12}]=[A]\left\{-[\Omega_R][A_i]^T+[T_{12}]\int_{z_i}^{z}[A]^T\,\mathrm{d}z+[T_{22}]\left(\int_{z_i}^{z}[\Omega_R][A]^T\,\mathrm{d}z-[\Omega_R]\int_{z_i}^{z}[A]^T\,\mathrm{d}z\right)\right\}$

$[N_{13}]=[A][T_{13}]\int_{z_i}^{z}[A]^T\,\mathrm{d}z$

$[N_{14}]=[A]\left\{[T_{14}]\int_{z_i}^{z}[A]^T\,\mathrm{d}z+[T_{24}]\left(\int_{z_i}^{z}[\Omega_R][A]^T\,\mathrm{d}z-[\Omega_R]\int_{z_i}^{z}[A]^T\,\mathrm{d}z\right)\right\}$

$[N_{21}]=[0]$

$[N_{22}]=[A][T_{22}]\int_{z_i}^{z}[A]^T\,\mathrm{d}z$

$[N_{23}]=[0]$

$[N_{24}]=[A][T_{24}]\int_{z_i}^{z}[A]^T\,\mathrm{d}z$

3.2 The element stiffness matrix

The strain energy per unit length of pre-twisted Euler-Bernoulli beam under small deformation conditions is as follows

$$\Gamma=\iint_A\frac{1}{2}(\sigma_z\varepsilon_z+\tau_{z\xi}\gamma_{z\xi}+\tau_{z\eta}\gamma_{z\eta})\mathrm{d}\xi\mathrm{d}\eta \tag{25}$$

Based on the strain relations of the pre-twisted Euler-Bernoulli beam (Banerjee 2004, Chen *et al*. 2014, Chen *et al*. 2016)

$$\begin{cases}\gamma_{z\xi}=-\varphi_\eta+u'-kv-\eta\varphi_z'\\ \gamma_{z\eta}=\varphi_\xi+v'+ku+\xi\varphi_z'\\ \varepsilon_z=w'-\xi(\varphi_\eta'+k\varphi_\xi)+\eta(\varphi_\xi'-k\varphi_\eta)\end{cases} \tag{26}$$

and considering the following relations between internal force and stress (Chen *et al*. 2016)

$$\begin{bmatrix}N\\ Q_\xi\\ Q_\eta\end{bmatrix}=\iint_A\begin{bmatrix}\sigma_z\\ \tau_{z\xi}\\ \tau_{z\eta}\end{bmatrix}\mathrm{d}\xi\mathrm{d}\eta$$
$$\begin{bmatrix}M_z\\ M_\xi\\ M_\eta\end{bmatrix}=\iint_A\begin{bmatrix}\xi\tau_{z\eta}-\eta\tau_{z\xi}\\ \eta\sigma_z\\ -\xi\sigma_z\end{bmatrix}\mathrm{d}\xi\mathrm{d}\eta \tag{27}$$

substituting equation (26) and (27) into (25), the strain energy can be obtained

$$\Gamma=\frac{1}{2}[\varepsilon]^T[N]+\frac{1}{2}[K]^T[M] \tag{28}$$

where

$$[\varepsilon]=\begin{bmatrix}\varepsilon\\ \gamma_\xi\\ \gamma_\eta\end{bmatrix},\quad[K]=\begin{bmatrix}k_z\\ k_\xi\\ k_\eta\end{bmatrix},\quad[N]=\begin{bmatrix}N\\ Q_\xi\\ Q_\eta\end{bmatrix},\quad[M]=\begin{bmatrix}M_z\\ M_\xi\\ M_\eta\end{bmatrix},$$
$$\begin{cases}\varepsilon=w'\\ \gamma_\xi=-\varphi_\eta+u'-kv\\ \gamma_\eta=\varphi_\xi+v'+ku\end{cases},\quad\begin{cases}k_\xi=\varphi_\xi'-k\varphi_\eta\\ k_\eta=\varphi_\eta'+k\varphi_\xi\\ k_z=\varphi_z'\end{cases}$$

Based on equivalent constitutive equation of the pre-twisted beam, the strain energy can be expressed as

$$\Gamma=\frac{1}{2}[\varepsilon]^T[B][\varepsilon]+\frac{1}{2}[K]^T[D][K] \tag{29}$$

where

$$[B]=\begin{bmatrix}EA & 0 & 0\\ 0 & GA & 0\\ 0 & 0 & GA\end{bmatrix},\ [\mathrm{D}]=\begin{bmatrix}GJ & 0 & 0\\ 0 & EI_\xi & 0\\ 0 & 0 & EI_\eta\end{bmatrix}$$

The total potential energy of the pre-twisted beam element based on energy principle is as follows

$$\Pi=\int_{z_i}^{z_{i+1}}\Gamma\mathrm{d}z-\int_{z_i}^{z_{i+1}}[\mathrm{U}]^{\mathrm{T}}[\mathrm{p}]\mathrm{d}z$$
$$-\int_{z_i}^{z_{i+1}}[\varphi]^{\mathrm{T}}[\mathrm{m}]\mathrm{d}z-[\mathrm{U}]^{\mathrm{T}}[\bar{\mathrm{p}}]\Big|_{z_i}^{z_{i+1}}-[\varphi]^{\mathrm{T}}[\bar{\mathrm{m}}]\Big|_{z_i}^{z_{i+1}} \tag{30}$$

where $[p]$, $[m]$, $[\bar{\mathrm{p}}]$, $[\bar{\mathrm{m}}]$ represent the linear distribution load vector, distribution moment load vector, node concentrated load vector and node concentrated moment vector, respectively. Equation (30) can be expressed as the following by substituting equation (22), (23) and (29) into (30)

$$\Pi = \int_{z_i}^{z_{i+1}} \frac{1}{2}[\varepsilon]^{\mathrm{T}}[\mathrm{B}][\varepsilon]\mathrm{d}z + \int_{z_i}^{z_{i+1}} \frac{1}{2}[K]^{\mathrm{T}}[D][K]\mathrm{d}z$$
$$-\int_{z_i}^{z_{i+1}}[U]^{\mathrm{T}}[p]\mathrm{d}z - \int_{z_i}^{z_{i+1}}[\varphi]^{\mathrm{T}}[m]\mathrm{d}z - [U]^{\mathrm{T}}[\bar{p}]\Big|_{z_i}^{z_{i+1}} - [\varphi]^{\mathrm{T}}[\bar{m}]\Big|_{z_i}^{z_{i+1}}$$
$$= \frac{1}{2}\begin{bmatrix}[U_i]\\ [\varphi_i]\\ [U_{i+1}]\\ [\varphi_{i+1}]\end{bmatrix}^T \left(\int_{z_i}^{z_{i+1}} [T]^T \begin{bmatrix}[B] & \\ & [D]\end{bmatrix}[T]\mathrm{d}z \begin{bmatrix}[U_i]\\ [\varphi_i]\\ [U_{i+1}]\\ [\varphi_{i+1}]\end{bmatrix} - \int_{z_i}^{z_{i+1}} [N]^T \begin{bmatrix}[\mathrm{p}]\\ [\mathrm{m}]\end{bmatrix}\mathrm{d}z - \begin{bmatrix}[\bar{\mathrm{p}}]\\ [\bar{\mathrm{m}}]\end{bmatrix}\Bigg|_{z_i}^{z_{i+1}} \right) \tag{31}$$

Based on the principle of minimum potential energy, the stiffness and equivalent node load matrix are obtained as

$$[k]^e = l_i[T]^T \begin{bmatrix}[B] & \\ & [D]\end{bmatrix}[T] \tag{32}$$

$$[R]^e = \int_{z_i}^{z_{i+1}} [N]^T \begin{bmatrix}[\mathrm{p}]\\ [\mathrm{m}]\end{bmatrix}\mathrm{d}z - \begin{bmatrix}[\bar{\mathrm{p}}]\\ [\bar{\mathrm{m}}]\end{bmatrix}\Bigg|_{z_i}^{z_{i+1}} \tag{33}$$

4. The example analysis and discussion

The analysis model for our example is a cantilever beam, whose length l is 6000mm; the cross-section is rectangular (Fig. 4): the height h is 500mm, the width is 200mm. The pre-twisted angle ω is 0.5π. The steel elastic modulus E is 2.0×10^5 *Mpa* and Poisson's ratio is 0.3. The concentrated force P is 50*k*N, and the self-weight of beam is not considered in this case. The load vectors in this example are $[\mathrm{p}]=[\mathrm{m}]=[\bar{\mathrm{m}}]=(0,0,0)^T$ and, $[\bar{\mathrm{p}}]=(0,-50e3,0)^T$.

4.1 The effect of element size of using ANSYS model

Based on the infinite approach method and ANSYS software, the finite element model is established. The element type is Beam188 (Fig.5), the warping degree of freedom is ignored (K1=0, Unrestrained), and a cubic form shape function is used (K3=3). As the beam188 is a Timoshenko beam element and to compare with above Euler-Bernoulli beam model, this paper amplifies the original shear stiffness (GA=7.692e9) through multiplication by the coefficient 10^5 (Fig.6).

The cubic form shape function chosen means that the analysis result is precise when considering the classic straight beam (ω=0). However, this method using the infinite approach has obvious rotation discretization errors when pre-twisted angle is not equal to zero (Fig.7), and more elements must be used to decrease this discretization error. Based on displacement results of the end of the beam (Fig.8), the deviation of displacement is very small and almost zero when number of elements n is greater than 20 for this analysis case.

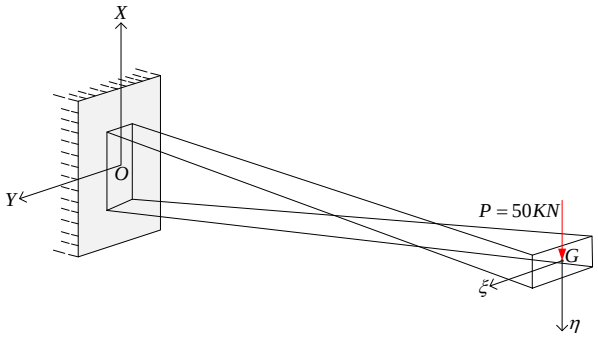

Fig. 4 The geometric parameter with rectangular cross section

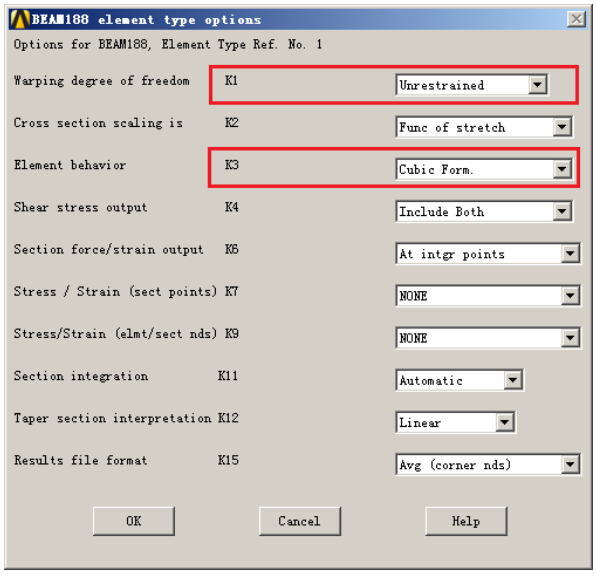

Fig. 5 The beam188 element type options

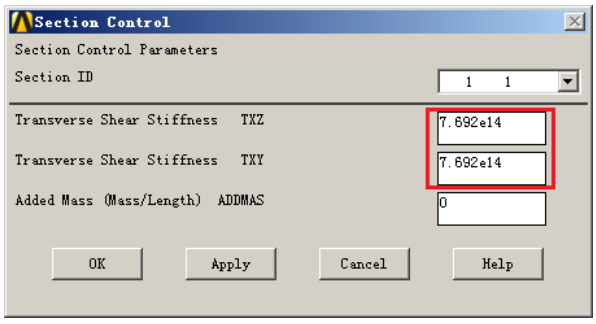

Fig. 6 The amplification of shear stiffness

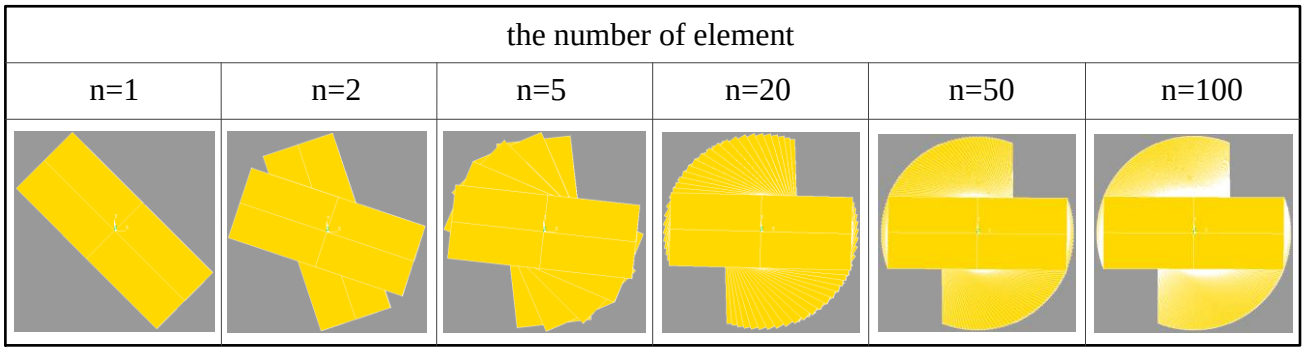

Fig. 7 The rotation discretization error ($\omega = 0.5\pi$)

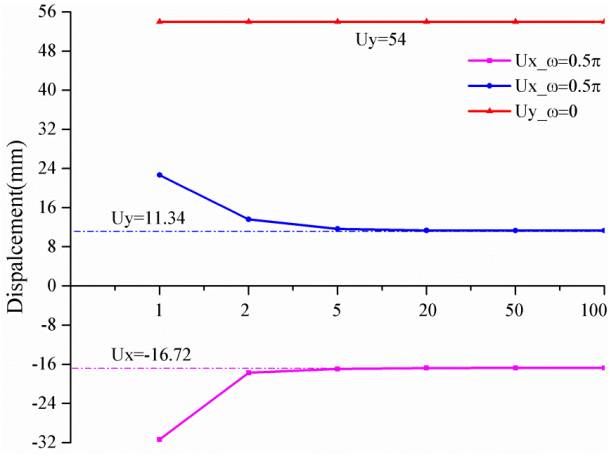

(a) the linear displacement comparison at the end of beam

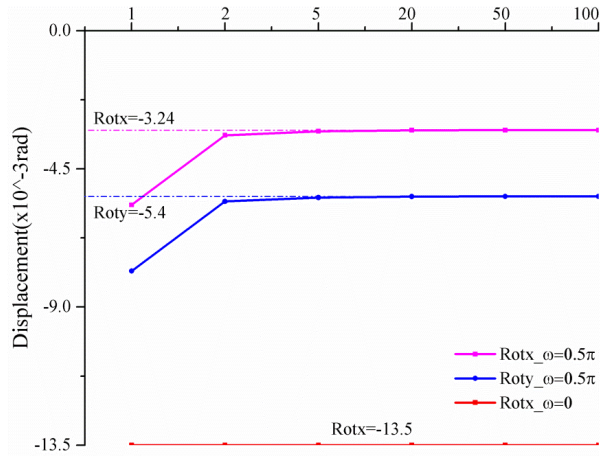

(b) the rotation displacement comparison at the end of beam

Fig. 8

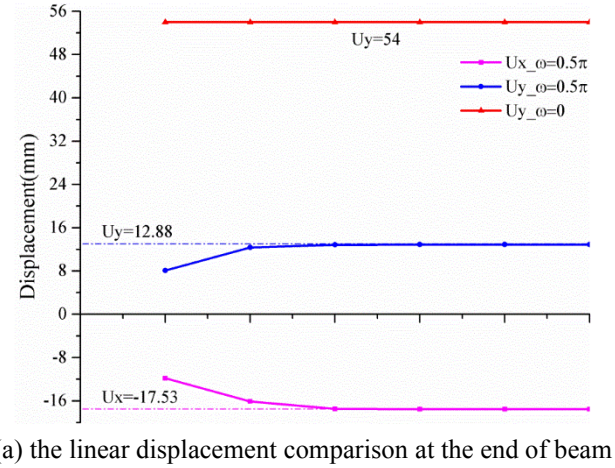

(a) the linear displacement comparison at the end of beam

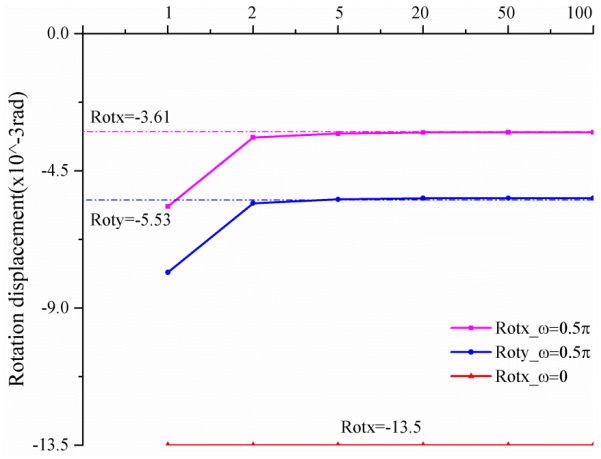

(b) the rotation displacement comparison at the end of beam

Fig. 9

4.2 The effect of element size of the proposed Euler-Bernoulli model

For further testing the effect of element size on results, the different element sizes of the proposed Euler-Bernoulli model will be used to validate this model; namely, the cantilever beam is divided into 1,2,5,20,50,100 equal parts, respectively. The displacement comparison results at the end of the beam are as shown in Fig.9, which also indicate that the deviation of displacement is very small and almost zero when the number of element n is greater than 20.

4.3 The effect of element size of the proposed model based on displacement general solution

The cantilever beam is divided into 1,2,5,20,50,100 equal parts. The displacement comparison results at the end of beam are as shown in Fig.10, which also indicates that the deviation of displacement is very small and almost zero when number of element n is greater than 20.

4.4 The comparison of displacement results

The displacement comparisons among the proposed Euler-Bernoulli model, the new numerical model based on

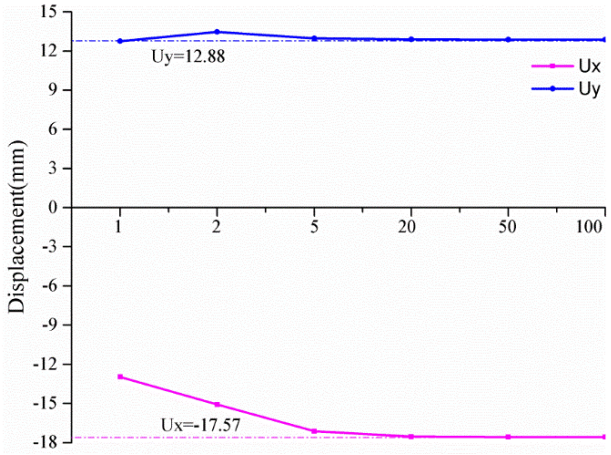

(a) the linear displacement comparison at the end of beam

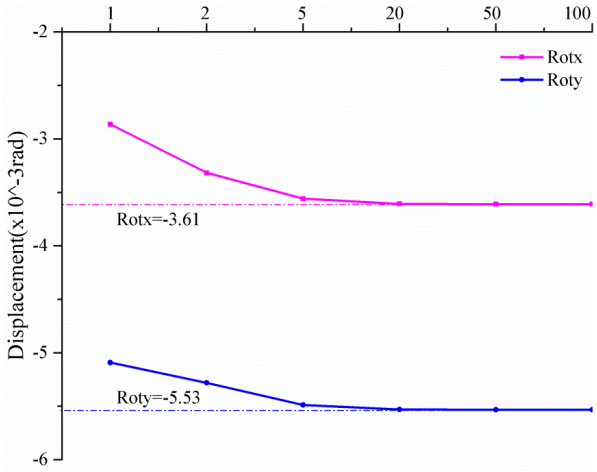

(b) the rotation displacement comparison at the end of beam

Fig. 10

displacement general solution, and ANSYS are as follows (Fig.11), where the number of elements used is 50.

The trends of displacement change are almost same among the proposed Euler-Bernoulli model, the new numerical model based on displacement general solution and the ANSYS model. Moreover, the results between the proposed Euler-Bernoulli model and the new numerical model based on displacement general solution are very close, and the curves are almost identical. The lateral displacements couple with each other; namely, the lateral linear displacement Uy and rotation displacement Roty will arise because of the existence of pre-twisted angle ω, as shown in Fig.11.

The deviation comparisons among these models are as follows. The deviations of Rotx and Roty are very small and less than 0.05% between the Euler-Bernoulli and proposed numerical model based on the displacement general solution, and the deviations of Ux and Uy are also small and less than 5%, except for the approximately the 1/6 areas the constraint end of the cantilever beam. Since the pre-twisted angle changes sharply from zero to $\omega/n = 0.5\pi/50$, the changes of deviation in this area are very large, but become smaller and smaller when farther away from the end of cantilever beam, as shown in Fig.12(a).

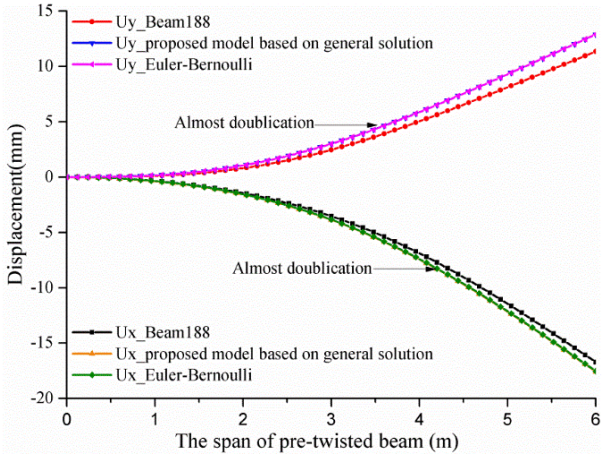

(a) the linear displacements comparison

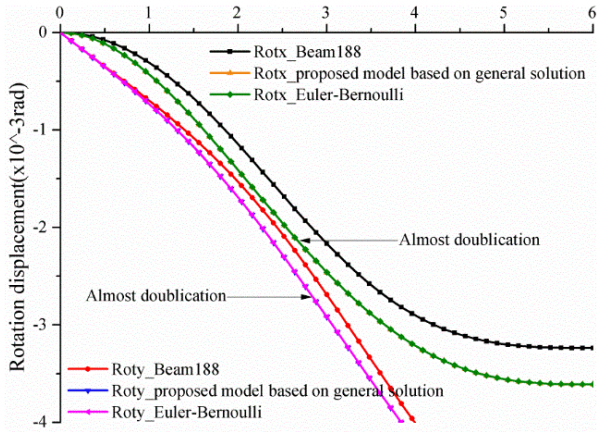

(b) the rotation displacements comparison

Fig. 11

The deviations between the Euler-Bernoulli and ANSYS model are larger than the above comparisons between the Euler-Bernoulli and proposed numerical model based on displacement general solution. The method by Beam188 element based on infinite approach to evaluate displacement is shown to be inaccurate (Fig.12b).

To further investigate the deviation error between the Euler-Bernoulli and ANSYS model, the comparison analysis by using different section sizes (200x200, 200x300, 200x400, and 200x500, respectively) are conducted. The results indicate that the displacement deviations will be smaller and smaller as the flexural stiffness along two main axis directions become closer and closer, as shown in Fig.13. This again indicates that the nature of the method based on infinite approach is just a decomposition of moment of inertia between the two main axial directions, and the nonlinear coupled effect is not considered.

4.5 The model further verification when pre-twisted angle is greater than π

To further verify the efficiency of the proposed model when pre-twisted angle is greater than π, the same case model in Fig.4 is also adopted, and only change the pre-twisted angle ω, as shown in Fig.14.

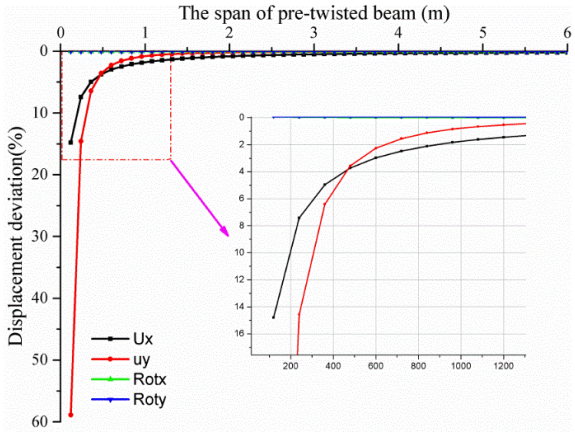

(a) the displacement deviation between ANSYS and the proposed numerical model based on general solution

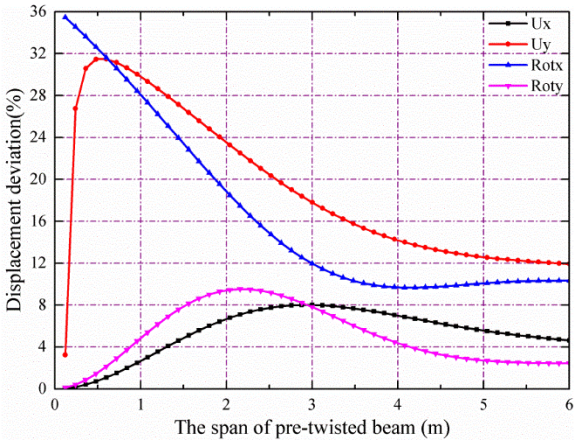

(b) the displacement deviation between Euler-Bernoulli and ANSYS model

Fig. 12

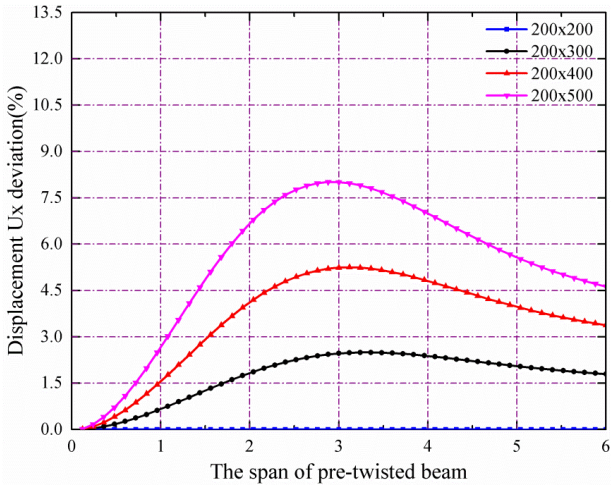

(a) the displacement Ux deviation comparison

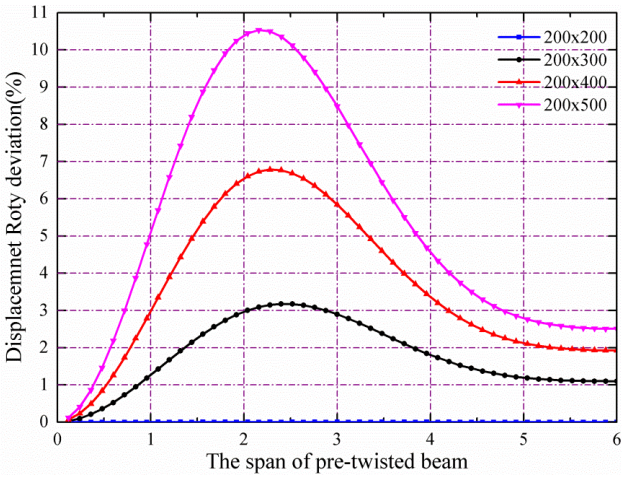

(b) the displacement Roty deviation comparison

Fig. 13

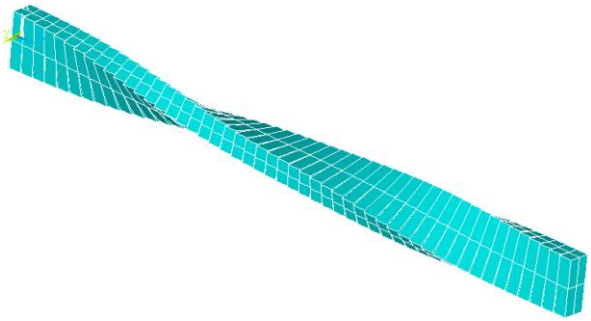

(a) the pre-twisted angle ω is equal to π

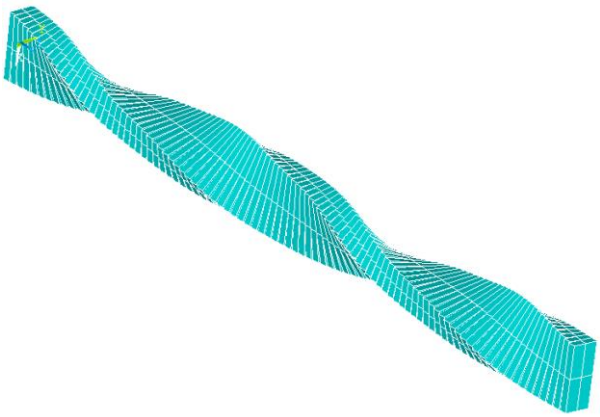

(b) the pre-twisted angle ω is equal to 2π

Fig. 14

The comparison results are developed, as shown in Fig.15. The proposed models in current work are still right when the pre-twisted angle ω is greater than π. The trends of displacement change are almost same among the proposed Euler-Bernoulli model, the new numerical model based on displacement general solution and the ANSYS model. Moreover, the results between the proposed Euler-Bernoulli model and the new numerical model based on displacement general solution are very close, and the curves are almost identical.

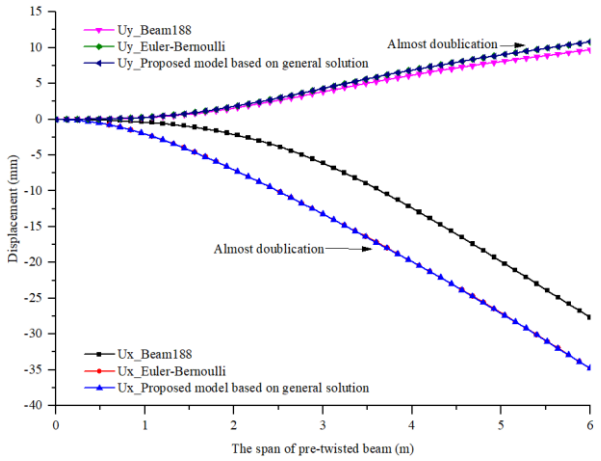

(a) the linear displacements Ux and Uy comparison with pre-twisted angle π

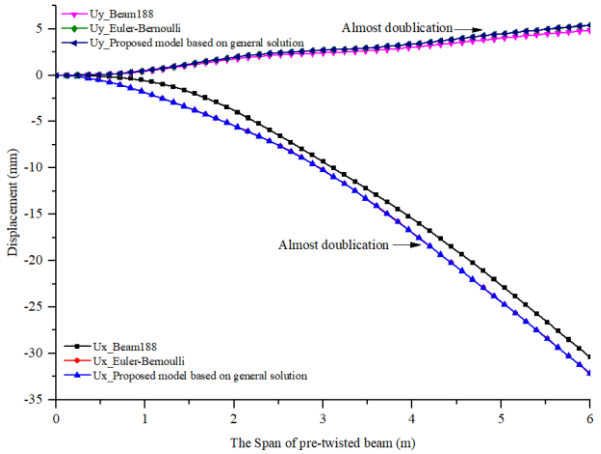

(b) the linear displacements Ux and Uy comparison with pre-twisted angle 2π

Fig. 15

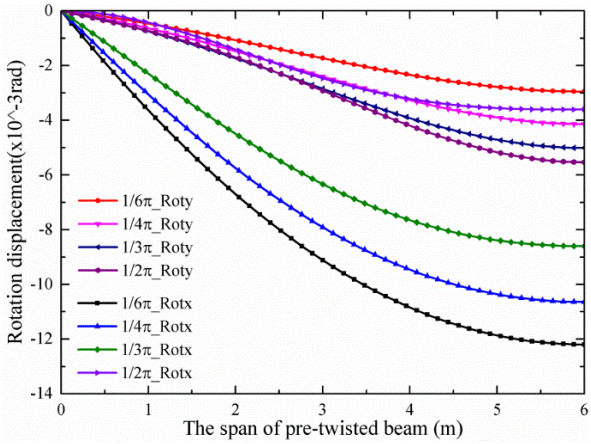

(a) the linear displacement comparison

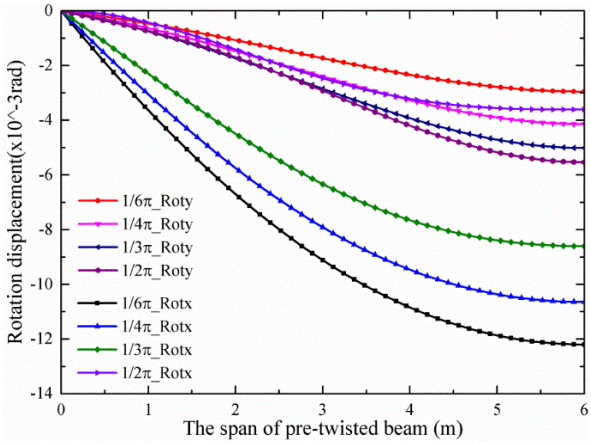

(b) the rotation displacement comparison

Fig. 16

5. Parametric analysis

5.1 The effect of pre-twisted angle on deflections

The effect of pre-twisted angle ω on the deflections has been investigated (Fig.16) and it is shown that the displacement Ux corresponding to the main axis $G\eta$ increased gradually with increasing of the pre-twisted angle, and the displacement Uy corresponding to the secondary axis $G\xi$ is also increased. The equivalent stiffness is also shown to be decreased along main axis direction as the increment of pre-twisted angle, and then the displacement is increased when the pre-twisted angle changes in the range of [0, 0.5π]. The displacements along main axis and secondary axis direction are coupled to each other because of the existence of pre-twisted angle. The coupling effect will become stronger, and the lateral displacement Uy will also be increased with the increasing of pre-twisted angle.

5.2 The effect of flexural stiffness ratio on deflections

The flexural stiffness ratio of pre-twisted beam with isotropic material is introduced as follows

$$\mu = \frac{I_\eta}{I_\xi} \geq 1 \tag{34}$$

Using the above example in the 4 section and assuming that the flexural stiffness EI_ξ along secondary axis $G\xi$ direction remains unchanged, the effect of the parameter μ on deflections has been investigated by changing the flexural stiffness ratio μ from 1 to 4 (Fig.17). The results show that the displacements Ux and Roty decreased corresponding to main axis $G\eta$, while the displacements Uy and Rotx increased corresponding to secondary axis $G\xi$ with the increasing of flexural stiffness ratio μ. The coupling effect of the pre-twisted beam becomes stronger between the strong axis and secondary axis as the flexural stiffness ratio μ increased.

6. Conclusions

1. Based on finite element method of the traditional straight Euler-Bernoulli beam, and using the coupled relations of pre-twisted Euler-Bernoulli beam between linear and angular displacements, the shape functions and stiffness matrix are deduced.

2. Based on the displacement general solution of a pre-

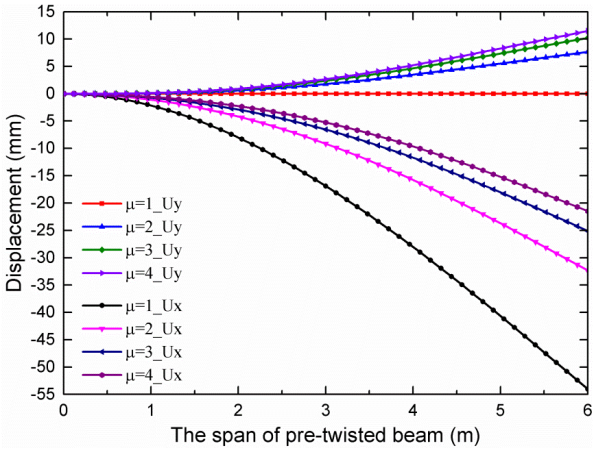

(a) the linear displacement comparison

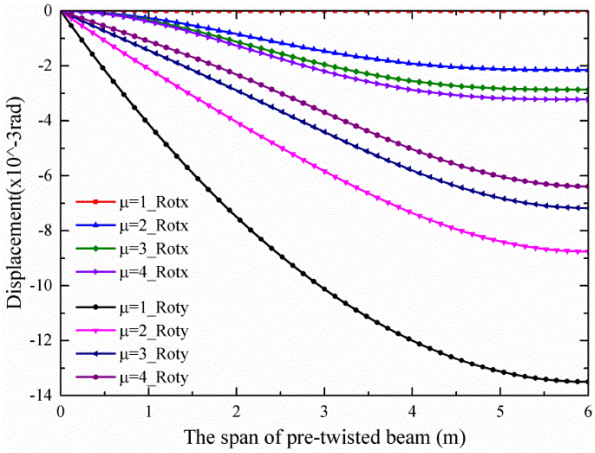

(b) the rotation displacement comparison

Fig. 17

twisted Euler-Bernoulli beam, the shape functions and stiffness matrix are deduced, and the precise finite element model is proposed.

3. By comparison with ANSYS solution by using Beam188 element based on infinite approach method, the results shows that the proposed models are available for pre-twisted Euler-Bernoulli beam and provide more accurate finite element models.

4. The effects of pre-twisted angle and flexural stiffness ratio on deflections have been investigated. The displacements along main axis and secondary axis directions are coupled to each other because of the existence of the pre-twisted angle. The equivalent flexural stiffness decreased along main axis direction as the increment of pre-twisted angle when the pre-twisted angle changes in the range of [0, 0.5π].

Acknowledgements

The authors would like to acknowledge the financial support by the National Natural Science Foundation of China (51408489, 51248007, 51308448 and 11572249), the China Scholarship Council (201606295016), and the Shaanxi National Science Foundation of China (2017JQ7255), and Sponsored by the Seed Foundation of Innovation and Creation for Graduate Students in Northwestern Polytechnical University (ZZ2019127).

References

Adair, D. and Jaeger, M. (2018), "Vibration analysis of a uniform pre-twisted rotating Euler–Bernoulli beam using the modified Adomian decomposition method", *Math. Mech. Solids*, **23**(9), 1345-1363. https://doi.org/10.1177/1081286517720843.

ANSYS Inc. (2016), ANSYS Programmer's Guide Release 18.0, 7th Ed., USA.

Banerjee, J. R. (2001), "Free vibration analysis of a twisted beam using the dynamic stiffness method", *J. Solids Structures*, **38**(38), 6703-6722. https://doi.org/10.1016/S0020-7683(01)00119-6.

Banerjee, J. R. (2004), "Development of an exact dynamic stiffness matrix for free vibration analysis of a twisted Timoshenko beam". *J. Sound Vib.*, **270**(1), 379-401. https://doi.org/10.1016/S0022-460X(03)00633-3.

Bahaadini, R. and Saidi, A. R. (2019), "Aero-thermoelastic flutter analysis of pre-twisted thin-walled rotating blades reinforced with functionally graded carbon nanotubes", *European J. Mech. A/Solids*, **75**, 285-306. https://doi.org/10.1016/j.euromechsol.2019.01.018.

Chen, J. and Li, Q. S. (2019), "Vibration characteristics of a rotating pre-twisted composite laminated blade", *Compos. Struct.*, **208**, 78-90. https://doi.org/10.1016/j.compstruct.2018.10.005.

Choi, S. C., Park, J. S. and Kim, J. H. (2007), "Vibration control of pre-twisted rotating composite thin-walled beams with piezoelectric fiber composites", *J. Sound Vib.*, **300**(1), 176-196. https://doi.org/10.1016/j.jsv.2006.07.051.

Chen, W. R. and Keer, L. M. (1993), "Transverse vibrations of a rotating twisted Timoshenko beam under axial loading", *J. Vib. Acoustics*, **115**(3), 285-294. https://doi.org/10.1115/1.2930347.

Chen, C. H., Zhu, Y. F., Yao, Y., Huang, Y. and Long, X. (2016), "An evaluation method to predict progressive collapse resistance of steel frame structures", *J. Constructional Steel Res.*, **122**, 238-250. https://doi.org/10.1016/j.jcsr.2016.03.024.

Chen, C. H., Yao, Y. and Huang, Y. (2014), "Elastic flexural and torsional buckling behavior of pre-twisted bar under axial load", *Struct. Eng. Mech.*, **49**(2), 273-283. https://doi.org/10.12989/sem.2014.49.2.273.

Chen, C. H., Zhu, Y. F., Yao, Y. and Huang, Y. (2016), "The finite element model research of the pre-twisted thin-walled beam", *Struct. Eng. Mech.*, **57**(3), 389-402. https://doi.org/10.12989/sem.2016.57.3.389.

Gu, X. J., Hao, Y. X., Zhang, W., Liu, L. T. and Chen, J. (2019), "Free vibration of rotating cantilever pre-twisted panel with initial exponential function type geometric imperfection", *Appl. Math. Model.*, **68**, 327-352. https://doi.org/10.1016/j.apm.2018.11.037.

Huang, Y., Chen, C., Zou, H. and Yao, Y. (2019), "The finite element model of pre-twisted Euler beam based on general displacement solution", *Struct. Eng. Mech.*, **69**(5), 479-486. https://doi.org/10.12989/sem.2019.69.5.479.

Huang, Y., Chen, C., Zou, H. and Yao, Y. (2019), "The finite element model of pre-twisted Euler beam based on general displacement solution", *Struct. Eng. Mech.*, **69**(5), 479-486. https://doi.org/10.12989/sem.2019.69.5.479.

Lee, J. Y. (2016), "Analysis of Vibration for the Pre-twisted Beam Considering the Effect of Rotary Inertia Using the Transfer Matrix Method", *Trans. Korean Soc. Noise Vib. Eng.*, **26**(2), 217-224. https://doi.org/10.5050/KSNVE.2016.26.2.217.

Mohanty, S. C., Dash, R. R. and Rout, T. (2015), "Vibration and dynamic stability of pre-twisted thick cantilever beam made of functionally graded material", *J. Struct. Stability Dynam.*, **15**(04), https://doi.org/10.1142/S0219455414500588.

Nabi, S. M. and Ganesan, N. (1996), "Comparison of beam and plate theories for free vibrations of metal matrix composite pre-twisted blades", *J. Sound Vib.*, **189**(2), 149-160. https://doi.org/10.1006/jsvi.1996.0012.

Oh, Y. and Yoo, H. H. (2018), "Vibration analysis of a rotating pre-twisted blade considering the coupling effects of stretching, bending, and torsion", *J. Sound Vib.*, **431**, 20-39. https://doi.org/10.1016/j.jsv.2018.05.030.

Rao, S. S. and Gupta, R. S. (2001), "Finite element vibration analysis of rotating Timoshenko beams", *J. Sound Vib.*, **242**(1), 103-124. https://doi.org/10.1006/jsvi.2000.3362.

Ramesh, M. N. V. and Rao, N. M. (2013), "Free vibration analysis of pre-twisted rotating FGM beams", *J. Mech. Mater. Design*, **9**(4), 367-383. https://doi.org/10.1007/s10999-013-9226-x.

Sinha, S. K. and Turner, K. E. (2011), "Natural frequencies of a pre-twisted blade in a centrifugal force field", *J. Sound Vib.*, **330**(11), 2655-2681. https://doi.org/10.1016/j.jsv.2010.12.017.

Shenas, A. G., Ziaee, S. and Malekzadeh, P. (2017), "Nonlinear vibration analysis of pre-twisted functionally graded microbeams in thermal environment", *Thin-Walled Struct.*, **118**, 87-104. https://doi.org/10.1016/j.tws.2017.05.003.

Shenas, A. G., Ziaee, S. and Malekzadeh, P. (2019), "Post-buckling and vibration of post-buckled rotating pre-twisted FG microbeams in thermal environment", *Thin-Walled Struct.*, **138**, 335-360. https://doi.org/10.1016/j.tws.2019.02.012.

Shenas, A. G., Malekzadeh, P. and Ziaee, S. (2017), "Vibration analysis of pre-twisted functionally graded carbon nanotube reinforced composite beams in thermal environment", *Compos. Struct.*, **162**, 325-340. https://doi.org/10.1016/j.compstruct.2016.12.009.

Wang, X. and Yuan, Z. (2018), "Three-dimensional vibration analysis of curved and twisted beams with irregular shapes of cross-sections by sub-parametric quadrature element method", *Comput. Math. Appl.*, **76**(6), 1486-1499. https://doi.org/10.1016/j.camwa.2018.07.001.

Yao, M., Niu, Y. and Hao, Y. (2019), "Nonlinear dynamic responses of rotating pre-twisted cylindrical shells", *Nonlinear Dynam.*, **95**(1), 151-174. https://doi.org/10.1007/s11071-018-4557-7.

Yoo, H. H., Kwak, J. Y. and Chung, J. (2001), "Vibration analysis of rotating pre-twisted blades with a concentrated mass", *J. Sound Vib.*, **240**(5), 891-908. https://doi.org/10.1006/jsvi.2000.3258.

Yu, A., Fang, M. and Ma, X. (2002), "Theoretical research on naturally curved and twisted beams under complicated loads", *Comput. Struct.*, **80**(32), 2529-2536. https://doi.org/10.1016/S0045-7949(02)00329-2.

Zhang, B., Zhang, Y. L., Yang, X. D. and Chen, L. Q. (2019), "Saturation and stability in internal resonance of a rotating blade under thermal gradient", *J. Sound Vib.*, **440**, 34-50. https://doi.org/10.1016/j.jsv.2018.10.012.

Zupan, D. and Saje, M. (2004), "On 'A proposed standard set of problems to test finite element accuracy': the twisted beam", *Finite Elements Analysis and Design*, **40**(11), 1445-1451. https://doi.org/10.1016/j.finel.2003.10.001.

Appendix A : The stiffness matrix of pre-twisted Euler-Bernoulli beam

$$
\mathbf{K}^e = EA\begin{bmatrix}
0&0&0&0&0&0&0&0&0&0&0&0\\
0&0&0&0&0&0&0&0&0&0&0&0\\
0&0&\frac{1}{l}&0&0&0&0&0&-\frac{1}{l}&0&0&0\\
0&0&0&0&0&0&0&0&0&0&0&0\\
0&0&0&0&0&0&0&0&0&0&0&0\\
0&0&0&0&0&0&0&0&0&0&0&0\\
0&0&0&0&0&0&0&0&0&0&0&0\\
0&0&0&0&0&0&0&0&0&0&0&0\\
0&0&0&0&0&0&0&0&0&0&0&0\\
0&0&-\frac{1}{l}&0&0&0&0&0&\frac{1}{l}&0&0&0\\
0&0&0&0&0&0&0&0&0&0&0&0\\
0&0&0&0&0&0&0&0&0&0&0&0
\end{bmatrix} + + GJ\begin{bmatrix}
0&0&0&0&0&0&0&0&0&0&0&0\\
0&0&0&0&0&0&0&0&0&0&0&0\\
0&0&0&0&0&0&0&0&0&0&0&0\\
0&0&0&0&0&0&0&0&0&0&0&0\\
0&0&0&0&0&0&0&0&0&0&0&0\\
0&0&0&0&0&\frac{1}{l}&0&0&0&0&0&-\frac{1}{l}\\
0&0&0&0&0&0&0&0&0&0&0&0\\
0&0&0&0&0&0&0&0&0&0&0&0\\
0&0&0&0&0&0&0&0&0&0&0&0\\
0&0&0&0&0&0&0&0&0&0&0&0\\
0&0&0&0&0&0&0&0&0&0&0&0\\
0&0&0&0&0&-\frac{1}{l}&0&0&0&0&0&\frac{1}{l}
\end{bmatrix}
$$

$$
+EI_\eta\begin{bmatrix}
\frac{53k^4l}{105}-\frac{8k^2}{5l}+\frac{12}{l^3} & \frac{11k^5l^2}{210}-\frac{6k^3}{5}+\frac{6k}{l^2} & 0 & \frac{k^3l}{3}-\frac{2k}{l} & \frac{11k^4l^2}{210}+\frac{k^2}{5}+\frac{6}{l^2} & 0 & \frac{83k^4l}{210}+\frac{8k^2}{5l}-\frac{12}{l^3} & -\frac{9k^5l^2}{140}+\frac{3k^3}{5}+\frac{6k}{l^2} & 0 & \frac{k^3l}{15}+\frac{2k}{l} & -\frac{9k^4l^2}{140}-\frac{4k^2}{5}+\frac{6}{l^2} & 0\\
\frac{11k^5l^2}{210}-\frac{6k^3}{5}+\frac{6k}{l^2} & \frac{k^6l^3}{105}-\frac{2k^4l}{15}+\frac{24k^2}{5l} & 0 & -\frac{7k^2}{5} & \frac{k^5l^3}{105}+\frac{k^3l}{15}+\frac{2k}{l} & 0 & \frac{9k^5l^2}{140}-\frac{3k^3}{5}-\frac{6k}{l^2} & -\frac{k^6l^3}{140}+\frac{k^4l}{3}+\frac{6k^2}{5l} & 0 & \frac{k^4l^2}{30}+\frac{3k^2}{5} & -\frac{k^5l^3}{140}+\frac{2k^3l}{15}+\frac{4k}{l} & 0\\
0&0&0&0&0&0&0&0&0&0&0&0\\
\frac{k^3l}{3}-\frac{2k}{l} & -\frac{7k^2}{5} & 0 & \frac{8k^2l}{15} & -k & 0 & \frac{k^3l}{15}+\frac{2k}{l} & -\frac{k^4l^2}{30}-\frac{3k^2}{5} & 0 & -\frac{2k^2l}{15} & -\frac{k^3l^2}{30}-k & 0\\
\frac{11k^4l^2}{210}+\frac{k^2}{5}+\frac{6}{l^2} & \frac{k^5l^3}{105}+\frac{k^3l}{15}+\frac{2k}{l} & 0 & -k & \frac{k^4l^3}{105}+\frac{4k^2l}{15}+\frac{4}{l} & 0 & \frac{9k^4l^2}{140}+\frac{4k^2}{5}-\frac{6}{l^2} & -\frac{k^5l^3}{140}+\frac{2k^3l}{15}+\frac{4k}{l} & 0 & \frac{k^3l^2}{30}+k & -\frac{k^4l^3}{140}-\frac{k^2l}{15}+\frac{2}{l} & 0\\
0&0&0&0&0&0&0&0&0&0&0&0\\
\frac{83k^4l}{210}+\frac{8k^2}{5l}-\frac{12}{l^3} & \frac{9k^5l^2}{140}-\frac{3k^3}{5}-\frac{6k}{l^2} & 0 & \frac{k^3l}{15}+\frac{2k}{l} & \frac{9k^4l^2}{140}+\frac{4k^2}{5}-\frac{6}{l^2} & 0 & \frac{53k^4l}{105}-\frac{8k^2}{5l}+\frac{12}{l^3} & -\frac{11k^5l^2}{210}+\frac{6k^3}{5}-\frac{6k}{l^2} & 0 & \frac{k^3l}{3}-\frac{2k}{l} & -\frac{11k^4l^2}{210}-\frac{k^2}{5}-\frac{6}{l^2} & 0\\
-\frac{9k^5l^2}{140}+\frac{3k^3}{5}+\frac{6k}{l^2} & -\frac{k^6l^3}{140}+\frac{k^4l}{3}+\frac{6k^2}{5l} & 0 & -\frac{k^4l^2}{30}-\frac{3k^2}{5} & -\frac{k^5l^3}{140}+\frac{2k^3l}{15}+\frac{4k}{l} & 0 & -\frac{11k^5l^2}{210}+\frac{6k^3}{5}-\frac{6k}{l^2} & \frac{k^6l^3}{105}-\frac{2k^4l}{15}+\frac{24k^2}{5l} & 0 & \frac{7k^2}{5} & \frac{k^5l^3}{105}+\frac{k^3l}{15}+\frac{2k}{l} & 0\\
0&0&0&0&0&0&0&0&0&0&0&0\\
\frac{k^3l}{15}+\frac{2k}{l} & \frac{k^4l^2}{30}+\frac{3k^2}{5} & 0 & -\frac{2k^2l}{15} & \frac{k^3l^2}{30}+k & 0 & \frac{k^3l}{3}-\frac{2k}{l} & \frac{7\omega^2}{5} & 0 & \frac{8k^2l}{15} & k & 0\\
-\frac{9k^4l^2}{140}-\frac{4k^2}{5}+\frac{6}{l^2} & -\frac{k^5l^3}{140}+\frac{2k^3l}{15}+\frac{4k}{l} & 0 & -\frac{k^3l^2}{30}-k & -\frac{k^4l^3}{140}-\frac{k^2l}{15}+\frac{2}{l} & 0 & -\frac{11k^4l^2}{210}-\frac{\omega^2}{5}-\frac{6}{l^2} & \frac{k^5l^3}{105}+\frac{k^3l}{15}+\frac{2k}{l} & 0 & k & \frac{k^4l^3}{105}+\frac{4k^2l}{15}+\frac{4}{l} & 0\\
0&0&0&0&0&0&0&0&0&0&0&0
\end{bmatrix}
$$

$$
+EI_\xi\begin{bmatrix}
\frac{k^6l^3}{105}-\frac{2k^4l}{15}+\frac{24k^2}{5l} & -\frac{11k^5l^2}{210}+\frac{6k^3}{5}-\frac{6k}{l^2} & 0 & \frac{k^5l^3}{105}+\frac{k^3l}{15}+\frac{2k}{l} & \frac{7k^2}{5} & 0 & -\frac{k^6l^3}{140}+\frac{k^4l}{3}+\frac{6k^2}{5l} & -\frac{9k^5l^2}{140}+\frac{3k^3}{5}+\frac{6k}{l^2} & 0 & -\frac{k^5l^3}{140}+\frac{2k^3l}{15}+\frac{4k}{l} & -\frac{k^4l^2}{30}-\frac{3k^2}{5} & 0\\
-\frac{11k^5l^2}{210}+\frac{6k^3}{5}-\frac{6k}{l^2} & \frac{53k^4l}{105}-\frac{8k^2}{5l}+\frac{12}{l^3} & 0 & -\frac{11k^4l^2}{210}-\frac{k^2}{5}-\frac{6}{l^2} & \frac{k^3l}{3}-\frac{2k}{l} & 0 & \frac{9k^5l^2}{140}-\frac{3k^3}{5}-\frac{6k}{l^2} & \frac{83k^4l}{210}+\frac{8k^2}{5l}-\frac{12}{l^3} & 0 & \frac{9k^4l^2}{140}+\frac{4k^2}{5}-\frac{6}{l^2} & \frac{k^3l}{15}+\frac{2k}{l} & 0\\
0&0&0&0&0&0&0&0&0&0&0&0\\
\frac{k^5l^3}{105}+\frac{k^3l}{15}+\frac{2k}{l} & -\frac{11k^4l^2}{210}-\frac{k^2}{5}-\frac{6}{l^2} & 0 & \frac{k^4l^3}{105}+\frac{4k^2l}{15}+\frac{4}{l} & k & 0 & -\frac{k^5l^3}{140}+\frac{2k^3l}{15}+\frac{4k}{l} & -\frac{9k^4l^2}{140}-\frac{4k^2}{5}+\frac{6}{l^2} & 0 & -\frac{k^4l^3}{140}-\frac{k^2l}{15}+\frac{2}{l} & -\frac{k^3l^2}{30}-k & 0\\
\frac{7k^2}{5} & \frac{k^3l}{3}-\frac{2k}{l} & 0 & k & \frac{8k^2l}{15} & 0 & \frac{k^4l^2}{30}+\frac{3k^2}{5} & \frac{k^3l}{15}+\frac{2k}{l} & 0 & \frac{k^3l^2}{30}+k & -\frac{2k^2l}{15} & 0\\
0&0&0&0&0&0&0&0&0&0&0&0\\
-\frac{k^6l^3}{140}+\frac{k^4l}{3}+\frac{6k^2}{5l} & \frac{9k^5l^2}{140}-\frac{3k^3}{5}-\frac{6k}{l^2} & 0 & -\frac{k^5l^3}{140}+\frac{2k^3l}{15}+\frac{4k}{l} & \frac{k^4l^2}{30}+\frac{3k^2}{5} & 0 & \frac{k^6l^3}{105}-\frac{2k^4l}{15}+\frac{24k^2}{5l} & \frac{11k^5l^2}{210}-\frac{6k^3}{5}+\frac{6k}{l^2} & 0 & \frac{k^5l^3}{105}+\frac{k^3l}{15}+\frac{2k}{l} & -\frac{7k^2}{5} & 0\\
-\frac{9k^5l^2}{140}+\frac{3k^3}{5}+\frac{6k}{l^2} & \frac{83k^4l}{210}+\frac{8k^2}{5l}-\frac{12}{l^3} & 0 & -\frac{9k^4l^2}{140}-\frac{4k^2}{5}+\frac{6}{l^2} & \frac{k^3l}{15}+\frac{2k}{l} & 0 & \frac{11k^5l^2}{210}-\frac{6k^3}{5}+\frac{6k}{l^2} & \frac{53k^4l}{105}-\frac{8k^2}{5l}+\frac{12}{l^3} & 0 & \frac{11k^4l^2}{210}+\frac{k^2}{5}+\frac{6}{l^2} & \frac{k^3l}{3}-\frac{2k}{l} & 0\\
0&0&0&0&0&0&0&0&0&0&0&0\\
-\frac{k^5l^3}{140}+\frac{2k^3l}{15}+\frac{4k}{l} & \frac{9k^4l^2}{140}+\frac{4k^2}{5}-\frac{6}{l^2} & 0 & -\frac{k^4l^3}{140}-\frac{k^2l}{15}+\frac{2}{l} & \frac{k^3l^2}{30}+k & 0 & \frac{k^5l^3}{105}+\frac{k^3l}{15}+\frac{2k}{l} & \frac{11k^4l^2}{210}+\frac{k^2}{5}+\frac{6}{l^2} & 0 & \frac{k^4l^3}{105}+\frac{4k^2l}{15}+\frac{4}{l} & -k & 0\\
-\frac{k^4l^2}{30}-\frac{3k^2}{5} & \frac{k^3l}{15}+\frac{2k}{l} & 0 & -\frac{k^3l^2}{30}-k & -\frac{2k^2l}{15} & 0 & -\frac{7k^2}{5} & \frac{k^3l}{3}-\frac{2k}{l} & 0 & -k & \frac{8k^2l}{15} & 0\\
0&0&0&0&0&0&0&0&0&0&0&0
\end{bmatrix}
$$